Geometric Topology & Visualizing 1-Manifolds

K. E. Jordan[1], L. E. Miller[2], T. J. Peters[3], and A. C. Russell[4]

[1] IBM Corporation, One Rogers St., Cambridge, MA 02142 kjordan@us.ibm.com
[2] University of Connecticut, Storrs, CT, 06269-2155 lance.e.miller@gmail.com
[3] University of Connecticut, Storrs, CT, 06269-2155 & Kerner Graphics, Inc., San Rafael, CA, 94912 tpeters@cse.uconn.edu
[4] University of Connecticut, Storrs, CT, 06269-2155 acr@cse.uconn.edu

Abstract: Ambient isotopic approximations are fundamental for correct representation of the embedding of geometric objects in $\mathbf{R}^3$, with a detailed geometric construction given here. Using that geometry, an algorithm is presented for efficient update of these isotopic approximations for dynamic visualization with a molecular simulation.

1 Approximation and Topology for Visualization

Figure 1(a) depicts a knot[5] and Figure 1(b) shows a visually similar protein model[6]. prompting two criteria for efficient algorithms for visualization:

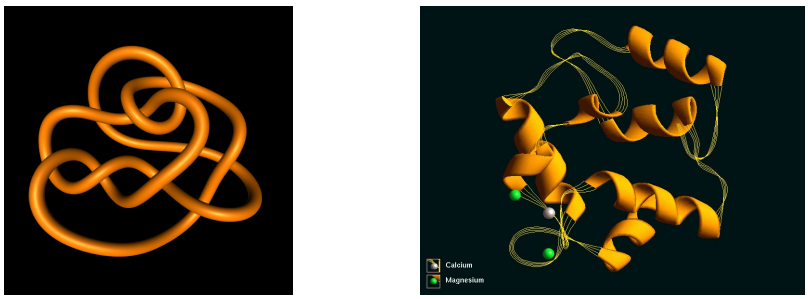

(a) (b)

Fig. 1. (a) Complicated Unknot (b) Protein-enzyme complex

– a piecewise linear (PL) approximation that preserves model topology,
– preservation of topology during dynamic changes, such as protein unfolding.

[5] Image credit: R. Scharein, www.knotplot.com
[6] Image credit: http://160.114.99.91/astrojan/protein/pictures/parvalb.jpg

The visual comparison from Figure 1 led to invoking knot theory to provide the unifying mathematics. This paper presents a curvature-adaptive, topology preserving approximation for a parametric 1-manifold with the primary result being Theorem 3. The piecewise linear (PL) approximations presented will

(i) be topologically equivalent to the original manifold,
(ii) minimize the number of linear approximants,
(iii) respect user-specified error bounds for distance & curvature.

While many approximation methods fulfill criteria (ii) and (iii), the stipulation of criterion (i) is of recent interest and the methods here are for a rich class of curves, extending related results. The topological equivalence chosen for dynamic molecular visualizations is by ambient isotopy, as this preserves the embedding of the geometric model over time.

Definition 1. *Let X and Y be two subsets of n-dimensional space $\mathbf{R}^n$. An* **ambient isotopy** *is a continuous function $H : \mathbf{R}^n \times [0,1] \to \mathbf{R}^n$ such that*

1. *$H(\cdot, 0)$ is the identity function,*
2. *$H(X, 1) = Y$, and*
3. *For each t in $[0,1]$, $H(\cdot, t)$ is a homeomorphism on $\mathbf{R}^n$.*

2 Related Work

Preliminary work by some of these authors and collaborators has appeared: for the integration of time and topology in animations and simulations [1] and for isotopic approximations on various classes of spline curves [2–5]. The theory presented here extends to a broad class of parametric curves that properly includes splines. While one approximation method could be applied to general parametric curves [1] the isotopy results within that paper relied upon Bézier geometry.

The proof techniques for isotopy here are a slight variant of the well-known 'push' from geometric topology for a 3-manifold [6]. The importance for applications is the creation of explicit neighborhoods within which the approximant can be perturbed while remaining ambient isotopic. These can serve as the basis for determining efficient updates for these isotopic constraints during dynamic visualizations.

A previous application of these tubular neighborhoods has emphasized visualizing knots undergoing dynamic changes [7]. Another tubular neighborhood algorithm [2] for rational spline curves [8] relies upon specialized numerical solution software, whereas computation with Newton's method has been exhibited on Bézier curves [3, 4]. Related treatments to curve approximations are available: within Hilbert spaces [9], with restrictions to planar curves [10] or specialized to spline curves [11]. The approach of approximating with respect to curvature is similar to an approach for 'aesthetic engineering' [12].

This terse summary on curve approximation stresses only the most relevant literature, as any comprehensive survey would be voluminous, with one indication being that a literature search on *curve approximation* resulted in 1.4 million

hits[7]. The distinguishing feature, here, is the additional insistence of topological equivalence. This emphasis upon geometric topology is appropriate when a geometric model is present, as for the molecular models discussed, and could prove complementary to other uses of topology in visualization that depend largely upon algebraic topology [13, 14].

3 Curvature & Topology for Parametric 1-Manifolds

Each curve considered here is assumed to be a compact 1-manifold, thereby excluding self-intersections, where stated differentiability assumptions also preclude wild arcs[8]. Further, each 1-manifold is assumed to have total arc length 1 and is parameterized over the unit[9] interval.

Notation: Let $c : [0,1] \rightarrow \mathbf{R}^3$ be a C^3 curve and we denote

$$\mu_c([a,b]) = \int_a^b ||c''(t)||dt,$$

which will be invoked as the basis for our curvature-adaptive approximation.

Theorem 1. *Let $c : [0,1] \rightarrow \mathbf{R}^3$ be a C^3 curve. For each $\varepsilon > 0$, there exists a natural number n and a partition $X = \{p_1, \ldots, p_n\} \subset [0,1]$ such that, for $i = 1, \ldots, n$, $p_1 = 0, p_n = 1$; $p_1 < p_2 \ldots < p_{n-1} < p_n$; and*

$$\int_{p_i}^{p_{i+1}} \|c''(z)\|dz = \mu_c([p_i, p_{i+1}]) < \varepsilon, \tag{1}$$

there is a set of compact cylinders $\{C_i\}_{i=1}^n$, such that each C_i has its axis aligned with the tangent at $c(p_i)$ and has radius ε. Furthermore both the polyline formed by consecutively connecting the vertices $\{c(p_i) : i = 1, \ldots, n\}$ and the curve c lie in $\bigcup_{i=1}^{n} C_i$.

Theorm 1 can be used to create a PL approximation of a curve, but there are no guarantees given that the approximant is topologically equivalent to the original curve. Further constraints must be imposed upon the choice of ε to ensure that the approximant produced is ambient isotopic to the original curve, as will be developed in the rest of this paper. The proof of Theorem 1 follows.

Proof. We construct one cylinder C_i for each point in the set X. Let L_i be the line containing the vector $c'(p_i)$. Consider the plane normal to $c'(p_{i+1})$. This plane intersects L_i at a point, denoted as q. Define C_i to be the cylinder of radius

[7] http://scholar.google.com/

[8] Any C^2 compact 1-manifold is tame [2].

[9] If not of unit length, scale accordingly.

ε whose axis is the portion of L_i connecting p_i and q. By Taylor's Theorem if $t \in [p_i, p_{i+1}]$ then

$$|c(t) - c(p_i) - (t - p_i)c'(p_i)| \leq \int_{p_i}^{t} ||c''(z)||(t-z)dz \leq \int_{p_i}^{p_{i+1}} ||c''(z)||dz < \varepsilon.$$

Hence, $c(t)$ is of distance at most ε from $c(p_i) + (t - p_i)c'(p_i)$. Thus $c(t)$ is at most ε away from L_i, and so $c(t)$ is in the cylinder C_i. The last statement is clear as each cylinder is convex and the endpoints $c(p_i), c(p_{i+1})$ of an approximating segment are contained in the cylinder C_i.

If, for each i, Inequality 1 is modified so that $\mu_c([p_i, p_{i+1}]) = \varepsilon$, then a previously published proof [1] can be applied for an asymptotic limit on the number of segments in the approximation. For $\varepsilon > 0$, denote by $N(\varepsilon)$ the number of cylinders given by the construction in the proof of Theorem 1.

Corollary 1. *If c is also C^3 such that $||c''(t)|| > 0$ for all t, then*

$$\lim_{\varepsilon \to 0} \sqrt{\varepsilon} \cdot N(\varepsilon) = \int_0^1 \sqrt{||c''(u)||}du.$$

We identify important properties studied in geometric topology and prove maintenance of those characteristics for the approximant. For the remainder of the section we will refer to the set $X = \{p_1, \ldots, p_n\}$ where the p_i's are ordered as described, above, and the cylinders C_i are constructed as in Theorem 1. We ensure that the curve is well-behaved within each cylinder through the following lemmas.

Lemma 1. *Let $c : [0, 1] \to \mathbf{R}^3$ be a C^3 curve and $r, s \in [p_i, p_{i+1}]$, then*

$$||c'(r) - c'(s)|| \leq \sqrt{3}\varepsilon.$$

Proof. For $t \in [0, 1]$ denote by $c'(t)_x$ the x-coordinate for $c'(t)$. We can apply Taylor's Theorem to see for $r, s \in [p_i, p_{i+1}]$,

$$|c'(r)_x - c'(s)_x| \leq \int_r^s |c''(u)_x|du \leq \int_r^s ||c''(u)||du \leq \varepsilon.$$

The case is similar for the y and z coordinates, and the result follows.

Corollary 2. *Let $c : [0, 1] \to \mathbf{R}^3$ be a C^3 space curve, and $\varepsilon < \sqrt{2/3}$. Then for points $r, s \in [p_i, p_{i+1}]$ the tangential deviation between $c'(r)$ and $c'(s)$ is no more than $\pi/2$.*

Proof. Since we are parameterized using arc length, we have $||c'(r)|| = ||c'(s)|| = 1$ for any $r, s \in [p_i, p_{i+1}]$. Further, by Lemma 1,

$$||c'(r) - c'(s)|| < \sqrt{3}\varepsilon.$$

The Law of Cosines shows the angle between them is $\arccos(1 - \frac{3}{2}\varepsilon^2)$. When $\varepsilon < \sqrt{\frac{2}{3}}$, we have $\arccos(1 - \frac{3}{2}\varepsilon^2) < \frac{\pi}{2}$.

So we can explicitly control the tangential deviation within each cylinder C_i. The benefit here is that we can use this information to control intersections within each cylinder.

Lemma 2. *Let $c : [0,1] \to \mathbf{R}^3$ be a C^3 curve and $[a,b] \subset [0,1]$. Assume all of the tangent vectors of the subcurve $c([a,b])$ deviate in angle by no more than $\eta < \frac{\pi}{2}$ from a particular tangent vector $c'(t)$ for $t \in [a,b]$. If Π is a plane with normal $c'(t)$ and $\Pi \cap c([a,b]) \neq \emptyset$, then $|c([a,b]) \cap \Pi| = 1$.*

Proof. Orient the plane Π so that it is parallel with the xy-plane and $c'(t)$ with the positive z-axis. In this orientation if $c'(r)_z = 0$ for any $r \in [a,b]$ then $c'(r)$ is parallel to the plane Π and this would be a contradiction as $c'(t)$ is normal to the plane Π and the angular deviation of tangent vectors is not more than $\frac{\pi}{2}$. For any $s \in [a,b]$ with $s \neq t$, if $c(s)$ lies on the plane Π then $c(s)_z = 0$ and since $c(t)_z = 0$ we have, by the Mean Value Theorem, another point r with $c'(r)_z = 0$, which is a contradiction.

Notation: For the remainder of this paper, let

- $c : [0,1] \to \mathbf{R}^3$ denote a C^3 curve,
- $\kappa = \max ||c''(z)||$, $\alpha = \min\{1, ||c''(z)||\}$,
- X be a set which satisfies the hypothesis of Theorem 1, and
- For $p_i, p_{i+1} \in X$, let $c_i = c([p_i, p_{i+1}])$.

Our next step is to construct sets upon which we can build local isotopies between the curve and the approximant. In order to do this we will make use of Taylor's theorem, as in the following lemma.

Lemma 3. *Let γ be chosen such that $\gamma > 0$, but $\gamma \ll (\kappa/2)(t-p_i)^2$. For $t \in (p_i, p_{i+1}]$, let S_t be the closed ball with center $c(p_i) + (t-p_i)c'(p_i)$ and radius r_t, with $r_t = (\kappa/2)(t-p_i)^2 + \gamma$. Then, $c(t) \in \text{int}(S_t)$.*

Proof. By Taylor's theorem we have

$$||c(t) - c(p_i) - (t-p_i)c'(p_i)|| \leq \int_{p_i}^{t} ||c''(z)||(t-z)dz$$
$$\leq \kappa[t^2 - (1/2)t^2 - (tp_i - (1/2)p_i^2)].$$

However $t^2 - (1/2)t^2 - (tp_i - (1/2)p_i^2) = (1/2)(t-p_i)^2$. The use of γ permits the conclusion about containment in the interior.

For each $t \in (p_i, p_{i+1}]$, define a 'snowcone' K_t as the convex hull[10] of S_t and $\{p_i\}$, where the use of the colloquial term 'snowcone' is meant to suggest the compact set created, with a planar cross-section shown in Figure 2. The next lemma shows the relationship between the opening angle of these snowcones[11] for different values t.

[10] For any two sets A and B, their convex hull is defined as the smallest convex set that contains $A \cup B$.

[11] In the United States, a frozen desert having a two dimensional profile similar to that of Figure 2 is known as a 'snowcone'.

Lemma 4. *Choose $\varepsilon \in (0, \alpha/(2\kappa))$. Let $t \in (p_i, p_{i+1}]$, let θ_t be opening angle at $c(p_i)$ for K_t. Then θ_t is an increasing function of t and each snowcone K_t, for $t \in (p_i, p_{i+1}]$, is contained in the snowcone $K_{p_{i+1}}$.*

Proof. Denote by $r_t = (\kappa/2)(t - p_i)^2$ the radius of S_t. Since

$$\int_{p_i}^{p_{i+1}} ||c''(z)||dz < \varepsilon$$

we have that $\alpha(p_{i+1} - p_i) < \varepsilon$ and since $\varepsilon < (2\alpha/\kappa)$ we have that

$$(t - p_i) \leq (p_{i+1} - p_i) \leq \varepsilon/\alpha \leq 2/\kappa.$$

Thus, $(\kappa/2)(t - p_i) \leq 1$ and $(\kappa/2)(t - p_i)^2 \leq (t - p_i)$. Therefore, $c(p_i)$ is not contained in the sphere S_t. Consider a planar cross section of the snowcone K_t and within this planar cross section, choose a tangent to S_t and denote the point of tangency as v. Denote the angle between $c'(p_i)$ and the segment $[c(p_i), v]$ by θ_t. Denote by z the center of S_t. Using the triangle defined by $z, v, c(p_i)$ one can conclude that $\sin\theta_t = r_t/(t - p_i) = (\kappa/2)(t - p_i)$. For reference, consider Figure 2. Since r_t is finite, $\theta_t < \pi/2$. For $t, s \in [p_i, p_{i+1}]$ with $t < s$, $\sin\theta_t < \sin\theta_s$ and so $\theta_t < \theta_s$, as $\theta_s < \pi/2$.

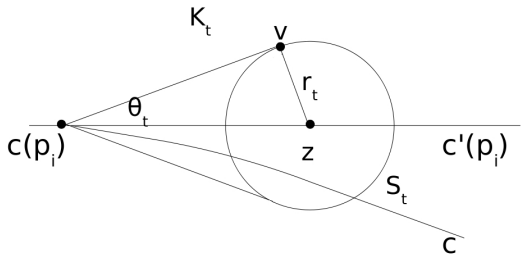

Fig. 2. Cross section of snowcone K_t

Hence, for $t \in (p_i, p_{i+1}]$, $K_t \subset K_{p_{i+1}}$.

Corollary 3. *The snowcone $K_{p_{i+1}}$ contains c_i.*

Proof. First note that $c(p_i) \in K_{p_{i+1}}$ as it is the apex of this snowcone. For each $t \in (p_i, p_{i+1}], c(t) \in K_{p_{i+1}}$ by Lemmas 3 and 4.

Notation: First, modify the existing notation $K_{p_{i+1}}$ to be $K_{i,i+1}$, using the order of these subscripts to express that the snowcone's apex is at p_i and opens towards p_{i+1}. This is to contrast it with a similar snowcone, denoted as $K_{i+1,i}$, which will have its apex as the point $c(p_{i+1})$, its axis as the line containing $c'(p_{i+1})$ *but* will open towards p_i, as indicated in Figure 3.

Lemma 5. *For each $i = 1, \ldots, n-1$, denote the approximating segment connecting the points $c(p_i)$ and $c(p_{i+1})$ by $a_{i,i+1}$. For each cylinder C_i, there is a convex subset of C_i, denoted $V_{i,i+1}$, containing c_i, such that*

$$V_{i,i+1} \cap V_{i+1,i+2} = c(p_{i+1}).$$

Proof. Define $V_{i,i+1} = K_{i,i+1} \cap C_i \cap K_{i+1,i}$. Since each of the intersecting sets is convex, it is clear that $V_{i,i+1}$ is convex. But then, since both $c(p_i)$ and $c(p_{i+1})$ are in $V_{i,i+1}$, it is clear that $a_i \subset V_{i,i+1}$. From Corollary 3, $c_i \subset V_{i,i+1}$.

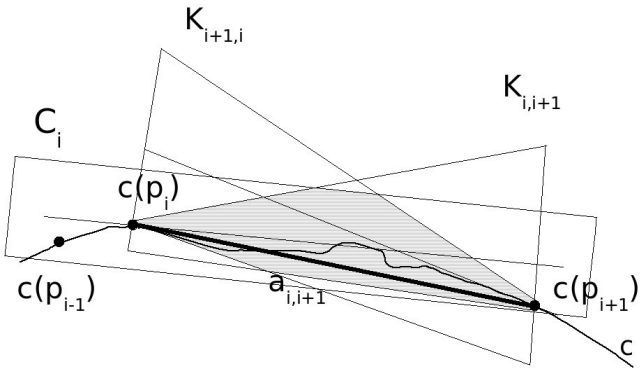

Fig. 3. Cross Section for bounding volume $V_{i,i+1}$

4 Building the Ambient Isotopy

The results so far only provide local views on c by focusing on each c_i independently. It is often easy to build an isotopy locally on one portion of a curve, but considerable subtlety can be required to unify these into an isotopy of the entire curve. The snowcones were defined for use in an iterative algorithm to establish an ambient isotopy for all of c.

Outline of Algorithm for Entire Curve: The geometric objective for the algorithm is to continue to reduce the radius of each cylinder C_i used in defining the sets $V_{i,i+1}$ until the interiors of these $V_{i,i+1}$ are pairwise disjoint, that is, for $i \neq j$,

$$int(V_{i,i+1}) \cap int(V_{j,j+1}) = \emptyset.$$

The algorithm begins with a seed value for δ to construct a set X_1 such that for each $i = 1, \ldots, n$, and $p_i, p_{i+1} \in X_1$, we have $\mu_c([p_i, p_{i+1}]) < \delta$. The algorithm proceeds by replacing the value of δ by $\delta/2$, so that at each successive iteration j, the set X_j has the above mentioned containment properties relative to the current value of δ. The algorithm proceeds until these bounding volumes are pairwise disjoint in order to form an isotopy of the entire curve. A previously published termination proof [3] can be easily modified for this snowcone geometry. Indeed, the more aggressive containment snowcone geometry used here actually simplifies the previous proof, so that both algorithms terminate in $O(\log \Delta^{-1})$ iterations [3], where Δ is the *minimum separation distance* of the curve. For the curve c, define $d : [0, 1] \to \mathbf{R}$ to be the distance function $d : (s, t) \mapsto \|c(s) - c(t)\|$. Then the minimum separation distance is the minimum critical value of d. A useful geometric formulation of this problem is to find all pairs of distinct points at parametric values s and t of c to satisfy the equations [15]:

$$(c(s) - c(t)) \cdot c'(s) = 0 \tag{2}$$

$$(c(s) - c(t)) \cdot c'(t) = 0. \tag{3}$$

Recent approaches to efficiently solve these simultaneous Equations 2 and 3 have appeared [3]. The value of Δ is then the minimum Euclidean distance over all pairs $(c(s), c(t))$ that are solutions to these simultaneous equations. The role of Δ as a stopping criterion can be intutitively expressed as measuring the minimum Euclidean distance between points of c that can be geodesically far apart. The algorithm restricts the size of the snowcones relative to Δ.

We first build a local homeomorphism on c_i and use that as a basis for constructing an ambient isotopy over all of c. For each point $w \in c_i$, let N_w denote the normal plane to c_i at w. Choose ϵ, in accordance with Corollary 2 to ensure that tangents on c_i deviate by less than $\pi/2$. Define the function

$$h_i : c_i \to a_{i,i+1}$$

by

$$h_i(w) \text{ is the single point in } N_w \cap a_{i,i+1}.$$

Theorem 2. *The function h_i is a homeomorphism that fixes both $c(p_i)$ and $c(p_{i+1})$.*

Proof. We consider the intersection of each N_w and $a_{i,i+1}$.

First, suppose that $a_{i,i+1}$ is a subset of N_w, requiring that both end points of $a_{i,i+1}$ were in N_w. But these end points are also points of c_i, which would be a contradiction to Lemma 2. If w is either endpoint of c_i, then it is also a point of $a_{i,i+1}$, but then Lemma 2 provides that this endpoint is the only element of the $N_w \cap a_{i,i+1}$.

So, suppose w is not an endpoint, then $c(p_i)$ cannot also be in N_w, by Lemma 2, and, similarly, $c(p_{i+1})$ cannot be in N_w. But, then, since $\pi/2$ is an upper bound on the tangents on c_i, it is clear that $c(p_i)$ and $c(p_{i+1})$ must be on

opposite sides of N_w. So, $a_{i,i+1}$ and N_w cannot be disjoint. But, then, N_w and $a_{i,i+1}$ intersect in a single point, since a plane and a line can intersect only in the line itself or in a single point.

Then h_i is a well-defined function on each c_i, where continuity is obvious. Moreover, note that h_i keeps the end points of c_i fixed. That h_i is onto follows since the endpoints of $a_{i,i+1}$ remain fixed and the image of h_i is a connected subset of $a_{i,i+1}$. That h_i is 1-1 follows, since $a_{i,i+1}$ is within ϵ of c_i, with ϵ chosen to be less than $1/(2\kappa)$ (with κ chosen to be the maximum curvature) so, the line segments given by $[w_1, h(w_1)]$ and $[w_2, h(w_2)]$ do not intersect.

Now we are set to define a local isotopy within the bounding volume $V_{i,i+1}$. But first we need to recall some easily proven properties of convex sets of $\mathbf{R}^n$. Let A denote a non-empty, compact, convex subset of $\mathbf{R}^n$, for some positive integer n.

Lemma 6. *For each point $p \in \text{int}(A)$ and $b \in \partial A$, the ray going from p to b only intersects ∂A at b (See Figure 4(a).)*

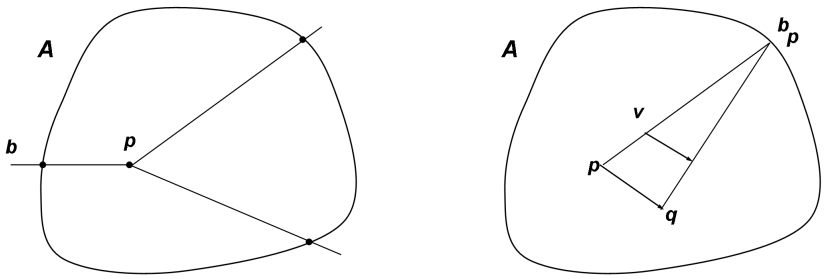

(a) (b)

Fig. 4. (a) Rays outward. (b) Variant of a push.

Lemma 7. *Let A be a compact convex subset of $\mathbf{R}^2$ with non-empty interior and fix $p \in int(A)$. For each boundary point $b \in \partial A$, denote by $[p, b]$ the line segment from p to b. Then $A = \bigcup_{b \in \partial A} [p, b]$.*

Many of the arguments of the proof of Theorem 2 can be adapted to build the ambient isotopy of c. The construction relies strongly on having a compact, convex set of support, as illustrated in Figure 4(b). The previous attention to convexity of $V_{i,i+1}$ was directed towards this construction.

Corollary 4. *There is an ambient isotopy of c_i, with compact support $V_{i,i+1}$ that takes each point of c_i to $h(c_i)$.*

Proof. A value of $\varepsilon > 0$ should be chosen so that $\varepsilon < \sqrt{2/3}$ to fulfill the conditions of Corollary 2 so that each h_i is a homeomorphism. Simultaneously choose, $\varepsilon < \alpha/(2\kappa)$ to satisfy the hypotheses of Lemma 4 while also constraining $\varepsilon \leq \delta$ to ensure that the interiors of the bounding volumes $V_{i,i+1}$ and $V_{j,j+1}$ are disjoint, with δ being the output of the iterative algorithm outlined at the beginning of this section. It should be clear that bounding volumes $V_{i,i+1}$ and $V_{i+1,i+2}$ intersect only at the point $c(p_{i+1})$.

The proof is a variant of a 'push' [6], where point p and q are in the interior of a non-empty, convex, planar set. As illustrated in Figure 4(b), each point v on a line segment between p and a boundary point b is mapped by linear interpolation onto the segment $[q, b]$, as p is mapped onto q, and then Lemmas 6 and 7 are applied to build the ambient isotopy from the homeomorphism of Theorem 2.

Theorem 3. *There is an ambient isotopy of c onto its PL approximant a and this isotopy has compact support $\bigcup_i V_{i,i+1}$.*

Proof. The snowcone construction leaves bounding volumes $V_{i,i+1}$ and $V_{i+1,i+2}$ intersecting only at the point p_{i+1}, which is fixed under the local isotopy, so a 'pasting lemma' [4] can be applied to complete the proof.

5 Conclusions and Future Work

The primary result of this work is a curvature-adpative, ambient isotopic approximation for a 1-manifold, inclusive of distance and tangency error bounds on the approximant. The bounding volumes also constrain many isotopic movements of the approximant curve.

The image of Figure 1(a) is the first frame of an animation showing that curve deforming under the application of energy described by Gaussian functionals, with guarantees that the embedded topology is preserved during this process. Similarly, the long-term focus here is to produce dynamic visualization of complex molecules undergoing simulated deformations under energy and chemical changes that also preserve the embedded topology. The essential first step is to produce a topology-preserving approximation of the static model. A specific approximated geometry model might be able to have multiple ambient isotopic perturbations within its bounding volume. However, if successive movements have the approximated geometry approaching the boundaries of the bounding volumes, new bounding volumes need to be computed. As long as the curve remains C^2 the existence of these new bounding volumes is known from classical differential topology [16].

However, those existence theorems typically do not provide explicit bounding geometry and they are not necessarily adaptive in the sense shown here. The value provided here is the detailed geometric constructions can be used to create algorithms that will allow for efficient updates of the geometric bounding neighborhoods as fundamental for dynamic visualization. The algorithm outlined in the second paragraph of Section 4 can be refined further, dependant upon the specific models being considered, for even more aggressive bounding

volumes, when geometric alternatives to the snowcones used here might be useful on specific data.

In Figure 1(b), there was considerable empty space around the geometric model being unfolded, but Figure 5 depicts a very dense configuration[12].

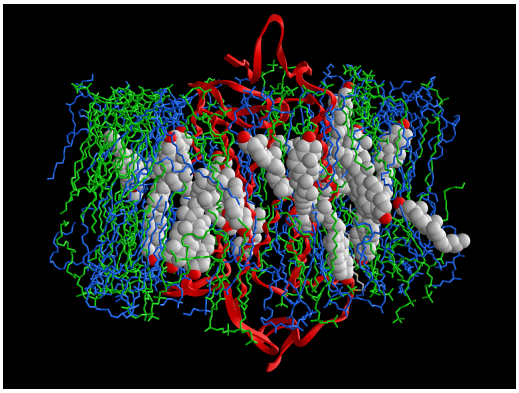

Fig. 5. Dense molecular configuration.

The control for isotopies can become quite delicate for molecular models. In Figure 5, the close geometric proximity and associated small bounding volumes will require updates after even small movements. This model has been the subject of consideration for dynamic visualization of molecular simulation [1] and is the current test case for algorithmic performance. The geometry in Figure 5 is also multi-dimensional, but the geometric topology used has well-known generalizations beyond dimension one. Guidance for extension to higher dimensions may be gained by considering other papers on topological approximation of 2-manifolds [17–20]. A particularly relevant comparison is to recent results focusing on a sufficiently dense set of sample points [19] to give both error bounds and topological guarantees.

6 Acknowledgements

All but the first author gratefully acknowledge partial support from NSF grant CCF 0429477. L. E. Miller & T. J. Peters express appreciation for additional support from IBM Doctoral Fellowships and an IBM Faculty Award during 2005 - 2008. All statements here are the responsibility of the authors, not of these funding sources. We thank the anonymous reviewers for many helpful suggestions.

[12] Image credit: http://domino.research.ibm.com/comm/pr.nsf/pages/rscd.bluegenepicaa.html.

References

1. Jordan, K.E., Miller, L.E., Moore, E.L.F., Peters, T.J., Russell, A.C.: Modeling time and topology for animation and visualization with examples on parametric geometry. Theoretical Computer Science **405** (2008) 41–49
2. Maekawa, T., Patrikalakis, N.M., Sakkalis, T., Yu, G.: Analysis and applications of pipe surfaces. Computer Aided Geometric Design **15**(5) (1998) 437–458
3. Miller, L., Moore, E.L.F., Peters, T.J., Russell, A.C.: Topological neighborhoods for spline curves : Practice & theory. Lecture Notes in Computer Science: Real Number Algorithms **5045** (2008) 149 – 161
4. Moore, E.L.F.: Computational Topology of Spline Curves for Geometric and Molecular Approximations. PhD thesis, The University of Connecticut (2006)
5. Moore, E.L.F., Peters, T.J., Roulier, J.A.: Preserving computational topology by subdivision of quadratic and cubic Bézier curves. Computing **79**(2) (2007) 317–323
6. Bing, R.H.: The Geometric Topology of 3-Manifolds. American Mathematical Society, Providence, RI (1983)
7. Cantarella, J., Piatek, M., Rawdon, E.: Visualizing the tightening of knots. In: VIS '05: Proceedings of the conference on Visualization '05, Washington, DC, USA, IEEE Computer Society (2005) 575–582
8. Piegl, L., Tiller, W.: The *NURBS* Book, 2nd Edition. Springer, New York, NY (1997)
9. Freedman, D.: Combinatorial curve reconstruction in Hilbert spaces: A new sampling theory and an old result revisited. Comput. Geom. **23**(2) (2002) 227–241
10. de Figueiredo, L.H., Stolfi, J., Velho, L.: Approximating parametric curves with strip trees using affine arithmetic. Comput. Graph. Forum **22**(2) (2003) 171–180
11. Peters, J., Wu, X.: On the optimality of piecewise linear max-norm enclosures based on slefes. In: Proceedings of Curves and Surfaces, St Malo 2002, Vanderbilt Press (2003)
12. Séquin, C.H.: CAD tools for aesthetic engineering. Computer-Aided Design **37**(7) (2005) 737–750
13. Cohen-Steiner, D., Edelsbrunner, H., Harer, J.: Stability of persistence diagrams. Discrete & Computational Geometry **37**(1) (2007) 103–120
14. Cohen-Steiner, D., Edelsbrunner, H., Harer, J., Morozov, D.: Persistent homology for kernels, images, and cokernels. In Mathieu, C., ed.: SODA, SIAM (2009) 1011–1020
15. Maekawa, T., Patrikalakis, N.M.: Shape Interrogation for Computer Aided Design and Manufacturing. Springer, New York (2002)
16. Hirsch, M.W.: Differential Topology. Springer-Verlag, New York (1976)
17. Amenta, N., Peters, T.J., Russell, A.C.: Computational topology: ambient isotopic approximation of 2-manifolds. Theoretical Computer Science **305**(1-3) (2003) 3–15
18. Boissonnat, J.D., Cohen-Steiner, D., Vegter, G.: Isotopic implicit surface meshing. In Babai, L., ed.: STOC, ACM (2004) 301–309
19. Clarkson, K.L.: Building triangulations using εs-nets. In Kleinberg, J.M., ed.: STOC, ACM (2006) 326–335
20. Dey, T.K., Edelsbrunner, H., Guha, S.: Computational topology. In: Advances in Discrete and Computational Geometry (Contemporary Mathematics 223, American Mathematical Society (1999) 109–143